

## Structural Characterizations of Charged Colloidal Silica Crystals Formed by Base Diffusion

Hiroshi Yamada,<sup>1,2</sup> Tsutomu Sawada,<sup>3</sup> Junpei Yamanaka,<sup>\*1</sup> Masakatsu Yonese,<sup>1</sup> and Fumio Uchida<sup>2</sup><sup>1</sup>Nagoya City University, 3-1 Tanabe, Mizuho, Nagoya 467-8603<sup>2</sup>Fuji Chemicals Co., Ltd., 1-35-1 Deyashiki-Nishi, Hirakata, Osaka 573-0003<sup>3</sup>National Institute for Materials Science, 1-1 Namiki, Tsukuba 305-0044

(Received September 20, 2007; CL-071043; E-mail: yamanaka@phar.nagoya-cu.ac.jp)

We examine the structures and orientation of charged colloidal silica crystals formed by the unidirectional diffusion of sodium hydrogencarbonate. Angular-dependent diffraction spectrometry is applied to centimeter-sized cubic crystals immobilized in polymer hydrogels. We find that the lattice planes of these crystals are not aligned with the container walls. This suggests that these large crystals are not formed by the wall effect, which has played a vital role in the formation of large crystals in previous studies.

Charged colloids undergo a phase transition from the disordered state to the ordered "crystal" state with an increase in the magnitude of electrostatic interparticle interaction.<sup>1</sup> In crystal states, colloidal particles are regularly arranged in body-centered cubic (bcc) or face-centered cubic (fcc) lattices. Since their Bragg wavelengths  $\lambda_B$  can be selected in the visible light regime, colloidal crystals have recently attracted considerable attention as photonic materials.<sup>2</sup> Hence, the applications of these crystals are severely restricted by their small sizes, the fabrication of large crystals has been studied extensively. In homogeneous colloids, millimeter- to centimeter-sized crystals are spontaneously formed under conditions near the crystallization phase boundary.<sup>3</sup> Thin crystals with large areas have been fabricated by various controlled crystallizations.<sup>4-7</sup> In most of these studies, container-wall effects have played a significant, or even indispensable role. The wall effects are important for the preparation of bulk colloids,<sup>3-5</sup> in addition to the preparation of close-packed opal film. In homogeneous colloids, the heterogeneous nucleation and growth of crystals on the container-wall result in the formation of large crystals;<sup>3</sup> in both shear annealing<sup>5</sup> and colloidal epitaxy,<sup>6</sup> the alignment of lattice planes along the container walls is a vital process. Usually, the closest-packed lattice planes ({110} and {111} planes for the bcc and fcc lattice structures, respectively) of these crystals are oriented parallel to the container wall.

In recent papers,<sup>8,9</sup> we have reported the unidirectional crystallization of charged colloidal silica by the diffusion of a base such as pyridine<sup>8</sup> and sodium hydrogencarbonate ( $\text{NaHCO}_3$ ).<sup>9</sup> The growth mechanism is attributed to a combination of the charging reaction of silica particles with increasing pH and charge-induced crystallization.<sup>10</sup> The maximum size of the resulting crystals is of the order of centimeters, and they have a pillar-like or cubic structure. In the present study, we examine the structures and orientation of the cubic crystals by applying a gel-immobilization technique and angular-dependent diffraction spectrometry.

Colloidal silica (particle diameter = 110 nm, particle volume fraction  $\phi = 0.0392$ ) was purified by dialysis and ion-exchange methods using a procedure reported elsewhere.<sup>9a</sup>

The purified silica colloid was disordered; however, it exhibited crystallization after the addition of ca. 15  $\mu\text{M}$   $\text{NaHCO}_3$ . The growth experiments were conducted using the experimental setup shown in Figure 1, whose details were reported earlier.<sup>9b</sup> The silica colloid was introduced into a poly(methyl methacrylate) cell ( $1 \times 1 \times 4.5 \text{ cm}^3$ ) and set in contact with a reservoir of aqueous  $\text{NaHCO}_3$  solution (500 mL,  $[\text{NaHCO}_3] = 60 \mu\text{M}$ ) through a semipermeable gel membrane to allow crystal growth. Gelation reagents, *N*-methylolacrylamide (gel monomer), *N,N'*-methylenebisacrylamide (crosslinker), and 2,2'-azobis[2-methyl-*N*-(2-hydroxyethyl)propionamide] (photoinduced radical polymerization initiator) were dissolved in both the silica colloid and  $\text{NaHCO}_3$  solution in the reservoir. The samples were grown for nearly 8 days at room temperature and gelled under UV-light illumination.

Figure 2 shows an overview of the gel-immobilized cubic crystal (ca.  $1 \times 1 \times 1 \text{ cm}^3$ ) that was cut from the original gelled sample; the four vertical planes (P1–P4) of the sample were in contact with the container-wall during the crystallization process. As indicated in Figure 2, hereafter, we use the orthogonal coordinate system with the origin at the center of the crystal; the *z* axis is along the growth direction, while the *x* and *y* axes are normal to the surface planes.

We determined the structure and lattice orientation of the crystal sample by detecting the Bragg conditions. The experimental system is illustrated in Figure 3. The sample was placed on the biaxial rotation stage with variable angles  $\theta_1$  and  $\theta_2$ . The values of  $\theta_1$  and  $\theta_2$  for the right-angle Bragg diffraction were determined by observing a back reflection with a macroscope. Subsequently, the reflectance spectrum from the lattice planes was measured by using a spectrophotometer (ImSpector, Kawasaki Steel Techno-research Co., Tokyo), from which a peak wavelength was read as a Bragg wavelength. In order to represent the lattice orientation, it is convenient to define an angle  $\alpha$  between the normal of the lattice plane and the closest coordinate axis (*x*, *y*, or *z* axis), as illustrated in Figure 3. We note that when the lattice planes are parallel to the cell wall, their

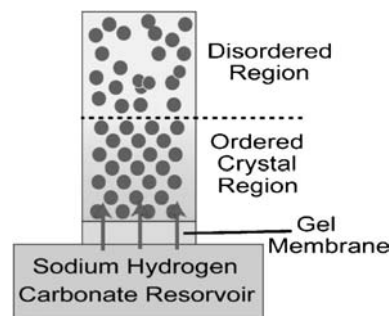
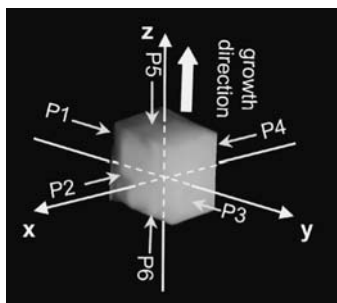
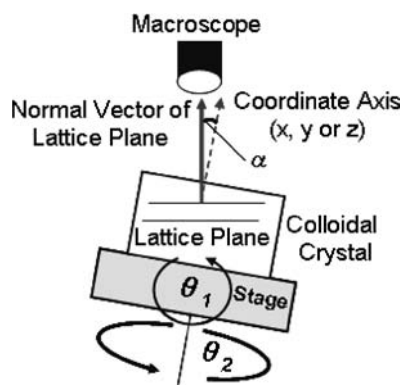


Figure 1. Schematic illustration of the crystal growth cell.



**Figure 2.** Gelled centimeter-sized cubic crystal and coordinate system.



**Figure 3.** Experimental setup to determine the lattice orientation of the crystal.

normal vectors should have the same directions as those for  $x$  or  $y$  axis (cf. Figure 2). In this case,  $\alpha = 0$  (cf. Figure 3). The  $\alpha$  value can be obtained through elemental calculation from the measured values of  $(\theta_1, \theta_2)$  by transforming the coordinate system with respect to the biaxial rotations. In this calculation, we considered the refraction at the sample/air interface based on Snell's law. The refractive index  $n$  of the colloidal crystal was assumed to be the volume-weighted average of the  $n$  values of all components (silica particles and water). We could examine the  $\alpha$  region ranging from 0 to 40°. The values of  $\lambda_B$  were corrected for slight swelling of the gelled sample during storage in water (5% on a length scale). We observed distinct Bragg diffraction from many lattice planes of the crystal. The observed Bragg conditions were localized at around  $(\lambda_B, \alpha) = \text{ca. } (597 \pm 23 \text{ nm}, 25.9 \pm 9.5^\circ; \text{region I})$  and  $\text{ca. } (438 \pm 10.3 \text{ nm}, 13.7 \pm 3.5^\circ; \text{region II})$ . Previous studies revealed that the colloidal crystal of silica particles with diameters of ca. 100 nm exhibits a bcc lattice structure at  $\phi \approx 0.03$ .<sup>8,9</sup> When the present crystal was assumed to have the bcc symmetry, the wavelengths of normal Bragg diffraction for the  $\{110\}$  and  $\{200\}$  lattice planes were calculated as  $\lambda_0 = 593 \text{ nm}$  and  $\lambda_0/\sqrt{2} = 419 \text{ nm}$ , respectively. In Figure 4, the  $\alpha$  values are plotted against the normalized Bragg wavelength  $\lambda \equiv \lambda_B/\lambda_0$ , where the solid and dotted lines represent the  $\{110\}$  ( $\lambda = 1$ ) and  $\{200\}$  ( $\lambda = 1/\sqrt{2}$ ) conditions, respectively. The  $\alpha$  values for the data represented by circles, squares, and triangles in Figure 4 are those calculated as angles between the normal vectors of each lattice planes and  $x$ ,  $y$ , and  $z$  axes, respectively.

It is apparent that the data points are scattered around the two lines. This indicates that the present large crystal had the

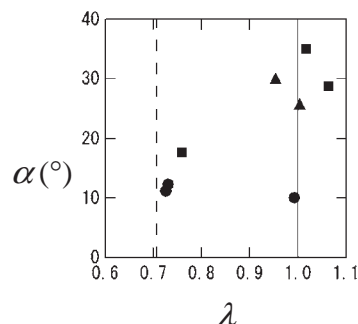


**Figure 4.** 90° Bragg wavelength  $\lambda$  and reflection orientation angle  $\alpha$  with respect to the closest coordinate axis.

bcc symmetry, as reported earlier. On the other hand, the  $\alpha$  values are significantly greater than 0°. The measurements for a different crystal sample showed  $(\lambda_B, \alpha) = (593 \pm 17 \text{ nm}, 12.4 \pm 8.7^\circ)$  in region I and  $(432 \pm 5.8 \text{ nm}, 30.5 \pm 2.8^\circ)$  in region II, which confirmed that  $\alpha$  value was not zero. These imply that neither the  $\{110\}$  nor the  $\{200\}$  lattice plane of the present crystal was oriented parallel to the cell wall. This is a rather surprising result because it indicates that the crystal was not formed by the wall effect. In previous findings,<sup>3,5,6</sup> the alignments of the lattice planes along the container walls are vital processes for the formation of large crystals. However, in the present growth system, we should consider a growth mechanism independent of the wall effect, which might be more intrinsic to the phenomenon of colloidal crystal growth. Further studies in this regard are in progress.

#### References

- 1 a) W. B. Russel, D. A. Saville, W. R. Schowalter, *Colloidal Dispersions*, Cambridge University Press, New York, **1989**. b) A. K. Sood, in *Solid State Phys.*, ed. by H. Ehrenreich, D. Turnbull, Academic Press, New York, **1991**. c) N. Ise, I. S. Sogami, *Structure Formation in Solution*, Springer, Berlin, **2005**.
- 2 J. Joannopoulos, R. Meade, J. Winn, *Photonic Crystals*, Princeton University Press, **1995**.
- 3 a) T. Okubo, *Langmuir* **1994**, *10*, 1695. b) T. Palberg, W. Mönch, J. Schwarz, P. Leiderer, *J. Chem. Phys.* **1995**, *102*, 5082. c) H. Yoshida, J. Yamanaka, T. Koga, T. Koga, N. Ise, T. Hashimoto, *Langmuir* **1999**, *15*, 2684.
- 4 a) M. Sullivan, K. Zhao, C. Harrison, R. H. Austin, M. Megens, A. Hollingsworth, W. B. Russel, Z. Cheng, T. Mason, P. M. Chaikin, *J. Phys.: Condens. Matter* **2003**, *15*, S11. b) A. van Blaaderen, *MRS Bull.* **2004**, *29*, 85.
- 5 a) N. A. Clark, A. J. Hurd, B. J. Ackerson, *Nature* **1979**, *281*, 57. b) A. Stipp, R. Biehl, T. Preis, J. Liu, A. B. Fontecha, H. J. Schöpe, T. Palberg, *J. Phys.: Condens. Matter* **2004**, *16*, S3885. c) T. Kanai, T. Sawada, A. Toyotama, K. Kitamura, *Adv. Funct. Mater.* **2005**, *15*, 25. d) A. Toyotama, T. Kanai, T. Sawada, J. Yamanaka, K. Ito, K. Kitamura, *Langmuir* **2005**, *21*, 10268.
- 6 a) A. van Blaaderen, R. Rene, P. Wiltzius, *Nature* **1997**, *385*, 321. b) J. P. Hoogenboom, A. Yethiraj, A. K. van Langen-Suurling, J. Romijn, A. van Blaaderen, *Phys. Rev. Lett.* **2002**, *89*, 256104.
- 7 A. Toyotama, J. Yamanaka, M. Yonese, T. Sawada, F. Uchida, *J. Am. Chem. Soc.* **2007**, *129*, 3044.
- 8 J. Yamanaka, M. Murai, Y. Iwayama, M. Yonese, K. Ito, T. Sawada, *J. Am. Chem. Soc.* **2004**, *126*, 7156.
- 9 a) N. Wakabayashi, J. Yamanaka, M. Murai, K. Ito, T. Sawada, M. Yonese, *Langmuir* **2006**, *22*, 7936. b) M. Murai, H. Yamada, J. Yamanaka, S. Onda, M. Yonese, K. Ito, T. Sawada, F. Uchida, Y. Ohki, *Langmuir* **2007**, *23*, 7510.
- 10 a) J. Yamanaka, T. Koga, N. Ise, T. Hashimoto, *Phys. Rev. E* **1996**, *53*, R4314. b) J. Yamanaka, H. Yoshida, T. Koga, N. Ise, T. Hashimoto, *Phys. Rev. Lett.* **1998**, *80*, 5806.